arTs Università degli Studi di Trieste
Archivio della ricerca – postprint

Unacylated ghrelin normalizes skeletal muscle oxidative stress and prevents muscle catabolism by enhancing tissue mitophagy in experimental chronic kidney disease

Gianluca Gortan Cappellari,* Annamaria Semolic,* Giulia Ruozi,† Pierandrea Vinci,* Gianfranco Guarnieri,* Francesca Bortolotti,† Davide Barbetta,‡ Michela Zanetti,* Mauro Giacca,† and Rocco Barazzoni*,[1]

*Department of Medical, Surgical, and Health Sciences, and ‡Animal Facility, University of Trieste, Trieste, Italy; and †Molecular Medicine Laboratory, International Centre for Genetic Engineering and Biotechnology, Trieste, Italy

ABSTRACT: Unacylated ghrelin (UnAG) may lower skeletal muscle oxidative stress, inflammation, and insulin resistance in lean and obese rodents. UnAG-induced autophagy activation may contribute to these effects, likely involving removal of dysfunctional mitochondria (mitophagy) and redox state maintenance. In chronic kidney disease (CKD) oxidative stress, inflammation and insulin resistance may negatively influence patient outcome by worsening nutritional state through muscle mass loss. Here we show in a 5/6 nephrectomy (Nx) CKD rat model that 4 d s.c. UnAG administration (200 μg twice a day) normalizes CKD-induced loss of gastrocnemius muscle mass and a cluster of high tissue mitochondrial reactive oxygen species generation, high proinflammatory cytokines, and low insulin signaling activation. Consistent with these results, human uremic serum enhanced mitochondrial reactive oxygen species generation and lowered insulin signaling activation in C2C12 myotubes while concomitant UnAG incubation completely prevented these effects. Importantly, UnAG enhanced muscle mitophagy *in vivo* and silencing RNA-mediated autophagy protein 5 silencing blocked UnAG activities in myotubes. UnAG therefore normalizes CKD-induced skeletal muscle oxidative stress, inflammation, and low insulin signaling as well as muscle loss. UnAG effects are mediated by autophagy activation at the mitochondrial level. UnAG administration and mitophagy activation are novel potential therapeutic strategies for skeletal muscle metabolic abnormalities and their negative clinical impact in CKD.—Gortan Cappellari, G., Semolic, A., Ruozi, G., Vinci, P., Guarnieri, G., Bortolotti, F., Barbetta, D., Zanetti, M., Giacca, M., Barazzoni, R. Unacylated ghrelin normalizes skeletal muscle oxidative stress and prevents muscle catabolism by enhancing tissue mitophagy in experimental chronic kidney disease.

KEY WORDS: autophagy · uremia · mitochondria

In chronic kidney disease (CKD), oxidative stress has been described in various tissues and at the whole-body level (1–8), possibly due at least in part to uremic toxins, the circulating levels of which increase as a result of reduced renal excretion (9). Reports in experimental models have shown that uremic toxins such as indoxyl sulfate greatly contribute to CKD-related muscle atrophy by increasing total skeletal muscle superoxide production and causing mitochondrial dysfunction, whereas uremic toxin inactivation may improve energy metabolism and muscle function (1, 10, 11). Oxidative stress may further synergistically enhance skeletal muscle catabolism and muscle mass loss by promoting tissue inflammation and insulin resistance, thereby contributing to worsened patient morbidity and mortality (2, 12, 13). Primary reactive oxygen species (ROS) sources and their potential regulators in CKD remain largely undefined, however. To our knowledge, to date, no studies are available on potential CKD-induced changes in skeletal muscle mitochondrial ROS production and their potential interaction with tissue inflammation, insulin signaling, and muscle weight.

Autophagy is a key intracellular degradation system, the generalized activation of which contributes to skeletal

ABBREVIATIONS: AG, acylated ghrelin; ATG5, autophagy protein 5; CKD, chronic kidney disease; COX, cytochrome *c* oxidase; GSK-3β, glycogen synthase kinase 3β; GSSG, oxidated glutathione; HUS, human uremic serum; IR, insulin receptor; IRS-1, insulin receptor substrate 1; LC3, microtubule-associated protein light chain 3; mTOR, mammalian target of rapamycin; Nx, 5/6 nephrectomy; P70S6K, ribosomal protein S6 kinase; PRAS40, proline-rich AKT substrate protein; ROS, reactive oxygen species; SAPK, stress-activated protein kinases; siRNA, silencing RNA; UnAG, unacylated ghrelin

[1] Correspondence: Department of Medical, Surgical, and Health Sciences, University of Trieste, Ospedale di Cattinara, Strada di Fiume 447, 34149 Trieste, Italy. E-mail: barazzon@units.it

muscle atrophy in various acute and chronic conditions (14–16). Autophagy activation at mitochondrial level (mitophagy), however, results in selective removal of damaged organelles and thereby reduces cell and tissue ROS production. Mitophagy is therefore an emerging relevant player in the maintenance of tissue redox state and metabolic homeostasis (17), and defective mitophagy in various tissues has been accordingly hypothesized to favor the onset of oxidative stress (18). No information is available on the potential impact of altered mitophagy in modulating CKD-induced skeletal muscle metabolic alterations.

Ghrelin is a gastric peptide hormone, the octanoylated form (acylated ghrelin, AG) of which is a major hypothalamic orexigenic signal (19–22). We previously demonstrated that AG may enhance skeletal muscle mitochondrial enzyme activities while reducing loss of body weight in experimental CKD in rodents (23), but sustained AG administration may lead to blood glucose elevation and unfavorable changes in cardiometabolic risk profile (24, 25). Higher total ghrelin levels are, however, interestingly associated with higher insulin-mediated glucose disposal and lower systemic inflammation in nondiabetic maintenance hemodialysis patients (26), and a more comprehensive understanding of the metabolic impact of ghrelin has been allowed by reports of independent metabolic effects of its unacylated form (UnAG). In particular, although no specific UnAG receptor has been yet identified (21), we recently showed that UnAG independently reduces skeletal muscle mitochondrial ROS generation (27), and UnAG-induced stimulation of whole-tissue autophagy was directly involved in this activity (17, 27, 28).

We therefore investigated *in vivo* and *in vitro* experimental CKD models (23, 29) to test 3 hypotheses: first, that CKD induces skeletal muscle mitochondrial dysfunction, as indicated by mitochondrial ROS overproduction and prooxidative redox state, proinflammatory changes in tissue cytokine patterns, and impaired insulin signaling activation with loss of muscle mass; second, that UnAG normalizes these abnormalities; and third, that UnAG activities are mediated by mitophagy activation. We consequently hypothesize that UnAG administration and mitophagy activation are novel potential strategies to limit CKD-induced skeletal muscle metabolic abnormalities and muscle loss.

MATERIALS AND METHODS

Experimental design and protocols

In vivo *uremic model and procedures*

Experimental protocol and surgery technique were approved by the Italian Ministry of Health Animal Experimentation Authority (DM 274/2013-B 07/11/2013) and were in adherence with National Institutes of Health (Bethesda, MD, USA) guidelines. A total of 40 male Wistar rats aged 12 wk (Harlan Industries, Indianapolis, IN, USA) were randomly assigned to 5/6 nephrectomy (Nx; $n = 30$) or sham surgery ($n = 10$). Throughout the whole study, rats were housed in individual cages with a 12-h light–dark cycle at the University Animal Facility, with water and standard rat chow (Harlan Industries 2018, 14.2 kJ/g) available *ad libitum*. Body weight and food intake were monitored twice a week. Surgery was performed *via* a single-step laparotomic approach (Supplemental Fig. 1) in order to reduce animal stress and complications. Procedures were performed under surgical sterility and anesthesia (premedication: dexmedetomidine 0.05 mg/kg, i.p., anesthesia: tiletamine/zolazepam [1:1] 25 mg/kg, i.p., local antalgic treatment: lidocaine 4mg/kg infiltration). After xiphopubic incision and median laparotomy, the left colon and part of the small bowel were mobilized and exteriorized in saline prewetted pads. The retroperitoneum was opened, and the inferior and superior left kidney poles were resected after clamping the renal artery. Hemostasis was assured by application of hemostatic absorbable sponge (Spongostan; Ethicon, Somerville, NJ, USA) and packing. After unclamping, the right kidney was also isolated with the same procedure and explanted after ligature of vessels and ureter. After accurate hemostasis check, packing was removed and the posterior peritoneum continuity reconstructed. The abdominal wall was reconstructed by mass-layer single absorbable stitch technique; the skin was sutured by single stitches. Sham-surgery animals underwent the same treatment except for kidney removal. During recovery, rats were monitored and treated twice a day for 3 to 6 d with saline solution (20 ml/kg/d, s.c.) and analgesic medication (tramadol, 5 mg/kg, s.c.) as necessary. Although no infectious complications were recorded, 20% of rats removed by chewing 2 or more cutaneous stiches, requiring medication twice a day. Ten days after surgery, all animals were free of any complications or treatment; 36 d after surgery, nephrectomized rats were randomly assigned to a 4 d, twice-daily subcutaneous saline (Nx, $n = 10$), AG (Nx-AG, $n = 10$), or UnAG (Nx-UnAG, $n = 10$) injection scheme (200 mg ghrelin/injection). UnAG and AG were synthesized by Bachem (Bubendorf, Switzerland). Sham-surgery animals were also treated with saline. After the last scheduled injection, food was removed and anesthesia was induced after 3 h (thiobutabarbital 100 mg/kg, tiletamine/zolazepam [1:1] 40 mg/kg, i.p.). Gastrocnemius and extensor digitorum longus muscles were then surgically isolated and blood collected by heart puncture.

In vitro *studies*

An *in vitro* model of uremia was reproduced by cell incubation with diluted uremic or control human plasma (30, 31). C2C12 myoblasts (ATCC CRL-1772) were differentiated into myotubes (32). After 4 d, after synchronization by starvation, cells were treated for 48 h with 10% (v/v) plasma added with heparin (final concentration 3 U/ml) and UnAG (1 μM), collected, and processed. An equimolar dose of AG was added in coincubation experiments. The potential role of autophagy in UnAG effects was assessed by silencing RNA (siRNA)-mediated genomic silencing of autophagy protein 5 (ATG5) or with nontargeting control siRNA #4 (both from GE Dharmacon, Lafayette, CO, USA) as previously described (27, 33). ATG5 protein level knockdown was verified by Western blot analysis.

Analytical methods

Plasma measurements

Plasma glucose, creatinine, and urea were determined by standard enzymatic–colorimetric assays.

Ex vivo *redox state*

ROS production in isolated intact mitochondria including both subsarcolemmal and intermyofibrillar subpopulations from both cells and tissue samples was measured using the Amplex Red (10 μM; Thermo Fisher Scientific, Waltham, MA, USA)–horseradish

peroxidase method as previously reported (27, 34) during an incubation of mitochondria at 37°C in different respiratory states. Results were normalized by citrate synthase activity in the same mitochondrial preparation. Final concentrations of substrates in the assay (mM) were: 8 glutamate, 4 malate, 10 succinate, 4 glutamate, 2 malate, 10 succinate, 0.05 palmitoyl-L-carnitine, 2 malate. Integrity of mitochondrial function was checked by verifying for each preparation the effects of carbonyl cyanide *m*-chlorophenyl hydrazone and antimycin A as well as ADP on H_2O_2 production because changes in mitochondrial activity after addition of these reagents are only possible in the presence of preserved mitochondrial function. *Ex vivo* mitochondrial and nonmitochondrial superoxide anion production in the gastrocnemius lateralis was assessed by the lucigenin chemiluminescent method in whole tissue homogenate (27, 34). Specific superoxide production from mitochondria was calculated as the reduction in light emission induced by the addition of mitochondrial uncoupling agent carbonyl cyanide *m*-chlorophenyl hydrazone (5 μM) to samples incubated with respiratory substrate succinate (10 mM). Superoxide generation from NADPH and xanthine oxidase was similarly calculated as the difference in light emission obtained by the addition of specific enzyme inhibitors on specific substrate-stimulated production rates (200 μM diphenyleneiodonium on 1 mM NADPH or 200 μM oxypurinol on 500 μM xanthine for NADPH or xanthine oxidase, respectively). Results were normalized by sample protein content [bicinchoninic acid (BCA) assay; Pierce, Rockford, IL, USA].

Total and oxidized glutathione

Tissue total and oxidized glutathione were determined as described elsewhere (27) on ~50 mg of gastrocnemius muscle. After sample cleaning and homogenization in ice-cold 5% (w/v) metaphosphoric acid (20 ml/g tissue), glutathione was measured spectrophotometrically as DTNB [5,5′-dithiobis-(2-nitrobenzoic acid) or Ellman reagent] conversion rate. Oxidated glutathione (GSSG) was measured after sample incubation with 2-vynilpiridin 10% (v/v) and neutralization by addition of triethanolamine 16.6% (v/v). Reduced glutathione was calculated as total minus GSSG.

Protein analyses

Cytokine profile and insulin signaling protein phosphorylation at insulin receptor ($IR^{Y1162/Y1163}$), insulin receptor substrate 1 ($IRS\text{-}1^{S312}$), AKT^{S473}, glycogen synthase kinase 3β ($GSK\text{-}3\beta^{S9}$), mTOR ($mTOR^{S2448}$), proline-rich AKT substrate protein ($PRAS40^{T246}$), ribosomal protein S6 kinase ($P70S6K^{T421/S424}$), p38/stress-activated protein kinases ($SAPK^{T180/Y182}$), MAPK/ERK $1/2^{T185/Y187}$, and $c\text{-}Jun^{S73}$ levels were measured by xMAP technology (Magpix; Luminex, Austin, TX, USA) using commercial kits (Life Technologies, Carlsbad, CA, USA) as described elsewhere (27). Data analysis was performed by Milliplex Analyst software (EMD Millipore, Billerica, MA, USA). Phosphorylation of insulin signaling mediators is expressed as phospho-protein units per total picogram of the same protein. Cytokine levels were normalized by protein content in homogenates as measured by bicinchoninic acid assay.

Tissue glucose uptake

Measurement of tissue glucose uptake was performed using the *ex vivo* nonradioactive 2-deoxyglucose method as described elsewhere (27). Two muscle sections were incubated for 30 min at 37°C under constant oxygenation with or without insulin (Humulin-R 600 pM) in isotonic buffer, added with bovine serum albumin (1 mg/ml) and pyruvate (2 mM). After a further 20 min incubation when pyruvate was substituted with 2-deoxyglucose (1 mM), samples were snap frozen and kept at −80°C. Quantification of 2-deoxyglucose-6-P in tissue homogenates was then performed using the method developed by Yamamoto *et al.* (35) by fluorometric measurement of resazurin conversion and normalized by protein concentration in sample homogenate. Tissue 2-deoxyglucose-6-P uptake was expressed in micromoles of 2-deoxyglucose/mg protein per 30 min.

Protein degradation marker analysis

Muscle proteolysis was assessed by measuring actin cleavage as the relative ratio of 14-kDa actin fragment over β-actin expression by Western blot analysis (36). Briefly, frozen gastrocnemius samples were homogenized and pellets with insoluble fraction resuspended in Laemmli buffer and separated by 12% PAGE under denaturing conditions. After transfer and antibody-mediated (A3853, 1:1000; Sigma-Aldrich, St. Louis, MO, USA) detection, densitometric analysis was performed and the results expressed as the ratio between optical densities of actin bands at 14 and 42 kDa.

Analysis of autophagy and mitophagy in skeletal muscle

Tissue samples were fixed in 4% formaldehyde and embedded in paraffin for immunofluorescence to highlight muscle fibers, autophagic flux, and mitophagy. After paraffin removal and tissue hydration, sections were permeabilized for 5 min in 0.1% Triton–PBS and blocked for 1 h with 5% bovine serum albumin in PBS; autophagic vesicles were stained with anti-microtubule-associated protein light chain 3 (LC3) B antibody (L7543, 1:200; Sigma-Aldrich) and anti–cytochrome *c* oxidase (COX) IV (ab33985, 1:200; Abcam, Cambridge, MA, USA). Alexa Fluor 594 donkey anti-rabbit (R37118, 1:500; Life Technologies) and Alexa Fluor 488 donkey anti-mouse (A-21202, 1:500; Thermo Fisher Scientific) were used as secondary antibodies. Endothelial cells were detected using FITC-conjugated lectin from *Triticum vulgaris* (L4895, 1:200; Sigma-Aldrich). Nuclei were stained with DAPI (H-1,200; Vector Laboratories, Burlingame, CA, USA). Cells were imaged using an Eclipse Ti confocal laser-scanning microscope (Nikon, Tokyo, Japan). The percentage of fibers showing numerous LC3 puncta was quantified to evaluate the autophagic response after different treatment. Five randomly chosen fields per tissue transversal section were quantified by ImageJ software (Image Processing and Analysis in Java; NIH; *http://imagej.nih.gov/*). To estimate the degree of colocalization of COX IV and LC3, Pearson's coefficient was calculated using the JACoP plug-in in ImageJ.

Statistical analysis

Groups were compared by the Student's *t* test, or in case of multiple comparisons, by 1-way ANOVA followed by appropriate *post hoc* tests. Bonferroni correction for multiple comparisons was applied. A value of $P < 0.05$ was considered statistically significant.

RESULTS

Animal characteristics and phenotype

As expected, Nx resulted in higher plasma creatinine and urea concentration (37), and exogenous 4 d UnAG

administration did not modify these parameters. Total calorie intake measured during the whole study period or during the 4-d UnAG or saline treatments was comparable in all groups. Physiologic increments in body weight and body mass index during the 40 d study period were impaired in both Nx groups compared to sham-surgery groups. Plasma glucose concentrations were comparable among Nx groups (**Table 1**).

Nx leads to high skeletal muscle mitochondrial ROS generation with proinflammatory cytokine changes, low insulin signaling, protein–catabolic changes, and loss of muscle mass

Compared to sham-surgery animals, untreated Nx had higher mitochondrial superoxide and H_2O_2 production as well as higher oxidized-to-total glutathione ratio, a validated marker of tissue redox state, the elevation of which indicates oxidative stress (**Fig. 1*A*–*E***). Interestingly, NADPH oxidase- and xanthine oxidase–mediated ROS production was also higher in the Nx group than in the sham-surgery group (Fig. 1*C*). Tissue cytokine patterns also shifted in Nx toward a proinflammatory profile with higher IL-1α, IL-1β, and TNF-α and lower antiinflammatory IL-10 (Fig. 1*F*). Nx decreased activating phosphorylation of insulin signaling proteins involved in glucose uptake activation (including AKT^{S473} and $GSK\text{-}3\beta^{S9}$; **Fig. 2*A***) and low insulin action was confirmed by low insulin-stimulated *ex vivo* muscle glucose uptake (Fig. 2*B*). Insulin-modulated protein anabolic signaling (mTOR, $PRAS40^{T246}$, and $P70S6K^{T421/S424}$) was notably also inhibited in Nx animals (**Fig. 3*A***), and activation of protein catabolism was further indicated by higher content of 14-kDa actin fragment, an established marker of muscle protein breakdown (36) (Fig. 3*B*). These clustered effects were notably associated with higher activating phosphorylation of inflammation-induced, uremia-associated master regulator of muscle protein homeostasis p38/SAPK (38, 39) as well as lower gastrocnemius muscle weight (Fig. 3*C*, *D*).

UnAG treatment normalizes Nx-induced metabolic abnormalities and muscle weight

Compared to Nx, Nx-UnAG animals had completely normalized skeletal muscle mitochondrial ROS generation and oxidized-to-total glutathione ratio (Fig. 1) despite lack of impact of NADPH and xanthine oxidases. UnAG treatment further normalized skeletal muscle cytokine patterns, insulin signaling protein activating phosphorylation, and insulin-stimulated muscle glucose uptake (Fig. 2). These effects were associated with reduced p38/SAPK phosphorylation and normalized gastrocnemius muscle weight (Fig. 3*C*, *D*).

UnAG increases activation of mitophagy in Nx skeletal muscle

To assess the *in vivo* impact of nephrectomy and UnAG on skeletal muscle autophagy and mitophagy, we analyzed the relative count of LC3-positive fibers in the gastrocnemius muscle by immunofluorescence. Nx enhanced autophagy but not mitophagy, thereby supporting a generalized activation of the autophagic process (**Fig. 4*A*, *B***) without selective targeting of mitochondrial homeostasis (Fig. 4*D*, *E*). UnAG further increased LC3-positive fibers and caused a substantial increment of mitophagy, thereby indicating that UnAG-induced autophagy activation predominantly occurs at mitochondrial level (Fig. 4*D*, *E*). c-Jun, an important activator of the autophagy regulator ATG5 involved in JNK-modulated autophagic and mitophagic pathways (40–43), was accordingly unaffected by Nx, but it was markedly higher in Nx animals treated with UnAG (Fig. 4*C*).

TABLE 1. *Animal characteristics*

Parameter	Time	Sham	Nx	Nx-UnAG
Body weight (g)	T0	364 ± 5^a	365 ± 7^a	365 ± 8^a
Δ Body weight (g)	T0–T40	94 ± 4^a	63 ± 4^b	72 ± 5^b
BMI (g/cm^2)	T0	0.66 ± 0.01^a	0.72 ± 0.04^a	0.67 ± 0.02^a
Δ BMI (g/cm^2)	T0–T40	0.11 ± 0.04^a	-0.04 ± 0.05^b	0.03 ± 0.02^b
WC (cm)	T0	18.3 ± 1.2^a	18.7 ± 0.3^a	18.2 ± 0.3^a
Δ WC (cm)	T0–T40	3.1 ± 0.6^a	0.2 ± 0.6^b	1.3 ± 0.2^c
Average food intake (g/d)	T0–T40	19.6 ± 0.4^a	20.2 ± 0.6^a	19.8 ± 0.5^a
Average food intake (g/d)	T36–T40	19.3 ± 0.5^a	20.1 ± 0.8^a	19.9 ± 0.6^a
Plasma glucose (mg/dl)	T40	122 ± 11^a	92 ± 6^b	94 ± 3^b
Plasma urea (mg/dl)	T40	21.54 ± 2.06^a	34.32 ± 0.96^b	30.96 ± 2.22^b
Plasma creatinine (μM)	T40	19.40 ± 0.87^a	27.82 ± 1.59^b	25.91 ± 1.00^b

Effects of 4 d unacylated (UnAG) ghrelin treatment (200 μg, s.c. injection twice a day) in Nx rats on body weight, body mass index (BMI), waist circumference at tissue collection, and their variation over time from surgery (Δ); average daily food intake after surgery and during UnAG or vehicle treatment; and plasma glucose, urea, and creatinine levels at tissue collection. $^{a,b,c}P < 0.05$ between groups with different letters for each parameter; means ± SEM, n = 8–10 per group.

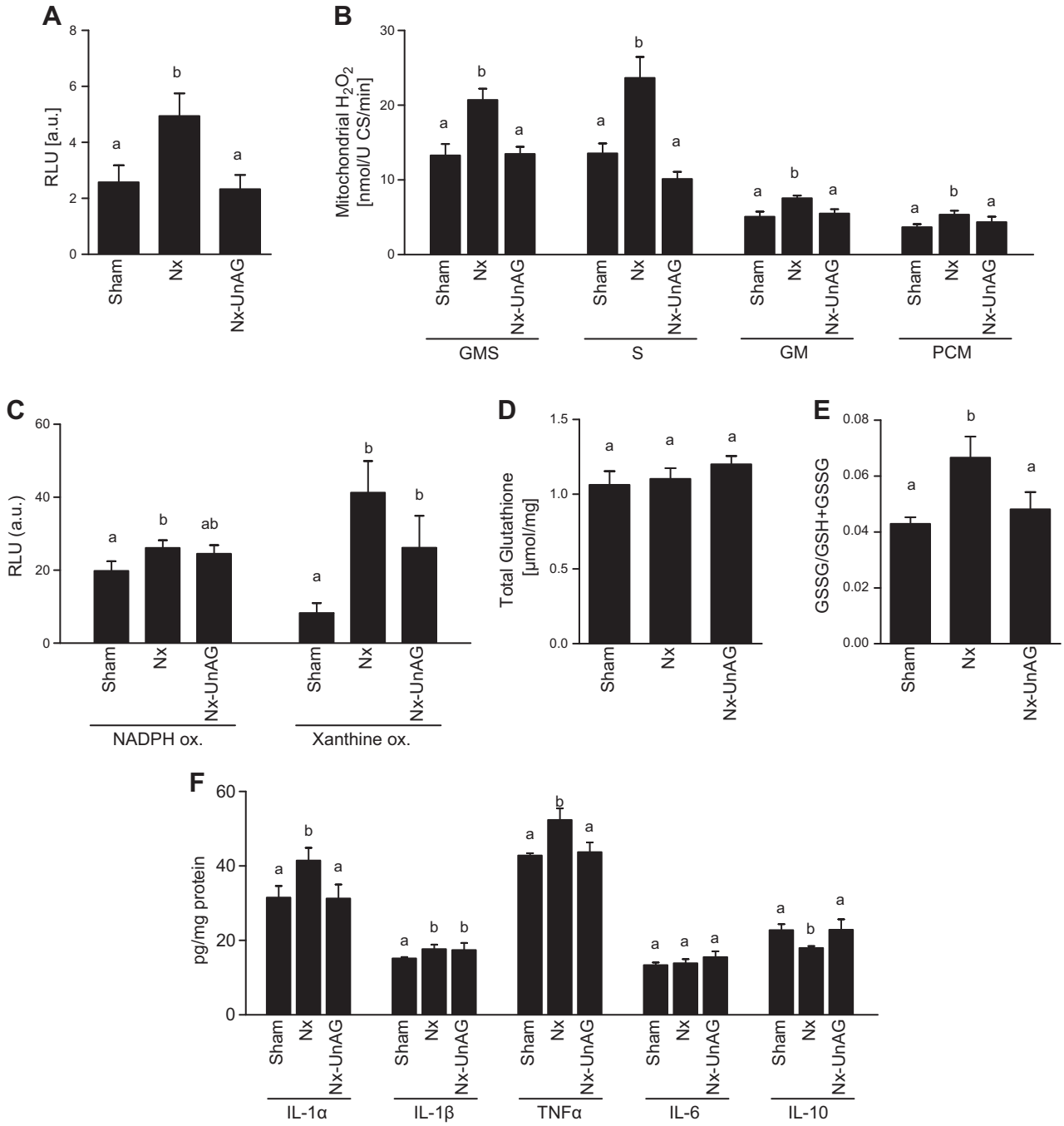

Figure 1. UnAG and skeletal muscle redox state and inflammation in Nx rats. *A*, *B*) Effects of 4 d of unacylated (UnAG) ghrelin treatment (200 µg, s.c. injection twice a day) in Nx rats on mitochondrial superoxide generation in gastrocnemius whole muscle tissue homogenate (*A*) and H_2O_2 production in intact isolated mitochondria with different respiratory substrates (*B*, GMS, glutamate + succinate + malate; S, succinate; GM, glutamate + malate; PCM, palmitoyl-L-carnitine + malate). *C–F*) Effects of UnAG treatment on superoxide production from NADPH and xanthine oxidases (*C*), total (*D*) and GSSG over total (*E*) tissue glutathione and on muscle expression of IL-1α, IL-1β, TNF-α, IL-6, and IL-10 measured by xMAP technology (*F*) in gastrocnemius muscle. A.u., arbitrary units; GSH, reduced gluthatione; RLU, relative light units; U CS, units of citrate synthase. Different letters (*a–c*) indicate $P < 0.05$ between groups; means ± SEM, n = 8–10 per group.

UnAG activities are independent of AG in Nx skeletal muscle

We next determined whether UnAG activities are independent of the acylated hormone form (AG). To exclude the possibility that UnAG-induced changes result from nonspecific activation of AG-regulated pathways, equimolar AG doses were administered to Nx animals under identical experimental conditions (n = 8; twice-daily 4 d 200 µg, s.c. AG). AG was unable to reproduce the effects of UnAG on skeletal muscle mitochondrial ROS production, inflammatory markers, insulin and protein

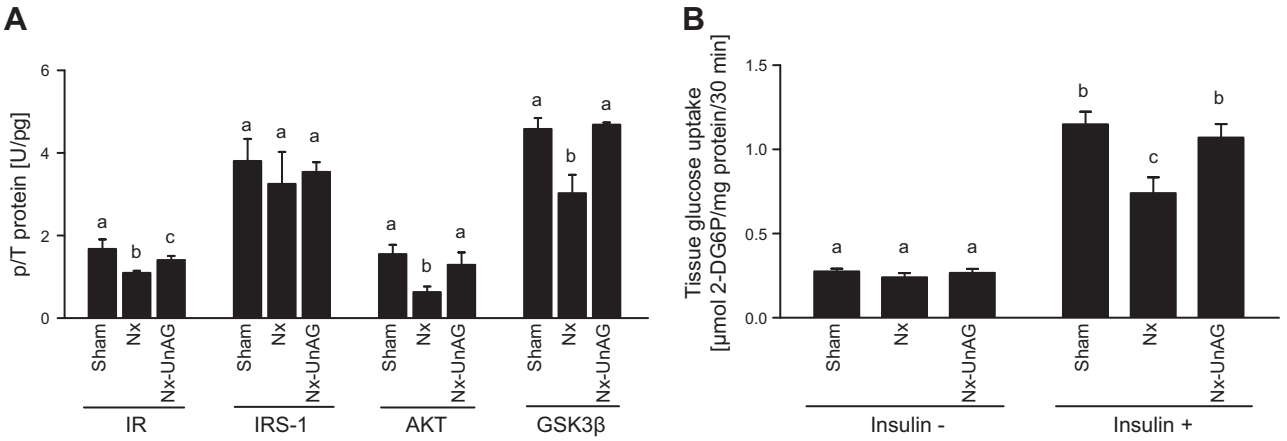

Figure 2. UnAG and skeletal muscle insulin action in Nx rats. Effects of 4 d UnAG (200 µg, s.c. injection twice a day) *vs.* saline (control, Ct) in Nx rats on gastrocnemius muscle relative phosphorylation of $IR^{Y1162/Y1163}$, $IRS\text{-}1^{S312}$, AKT^{S473}, and $GSK\text{-}3\beta^{S9}$ (*A*) and on extensor digitorum longus muscle glucose uptake in presence or absence of insulin coincubation (*B*). p/T, phosphoprotein to total protein ratio. Different letters (*a–c*) indicate $P < 0.05$ between groups; means ± SEM, $n = 8–10$ per group.

anabolic signaling, and glucose uptake as well as gastrocnemius muscle weight (**Fig. 5*A–I***). In addition, the impact of AG on both autophagy activation and mitophagy was markedly and statistically significantly lower than that of UnAG (Fig. 5*J–L* and Supplemental Figs. 2 and 3; all P = NS *vs.* Nx; $P < 0.05$ *vs.* UnAG).

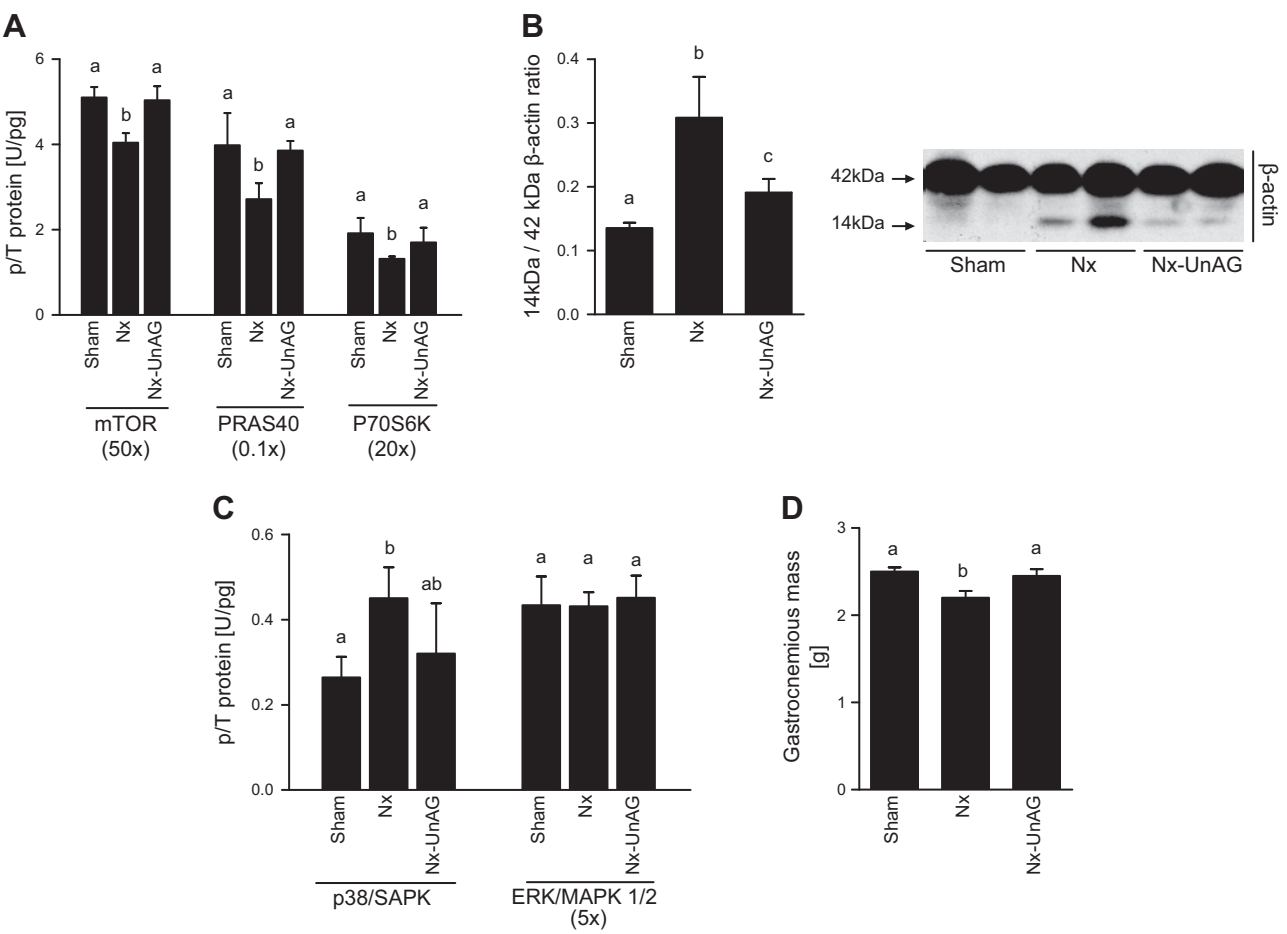

Figure 3. UnAG and skeletal muscle protein anabolic and catabolic pathways in Nx rats. Effects of 4-d UnAG (200 µg s.c. injection twice a day) *vs.* saline (control) in Nx rats on gastrocnemius muscle relative phosphorylation of $mTOR^{S2448}$, $PRAS40^{T246}$, and $P70S6K^{T421/S424}$ (*A*), on muscle 14-kDa actin fragment content, expressed as relative optical density over 42 kDa β-actin expression with representative blot (*B*), on relative phosphorylation of p38/SAPK $^{T180/Y182}$, MAPK/ERK $1/2^{T185/Y187}$ (*C*), and on gastrocnemius muscle mass (*D*). p/T, phosphoprotein to total protein ratio. Different letters (*a–c*) indicate $P < 0.05$ between groups; means ± SEM, $n = 8–10$ per group.

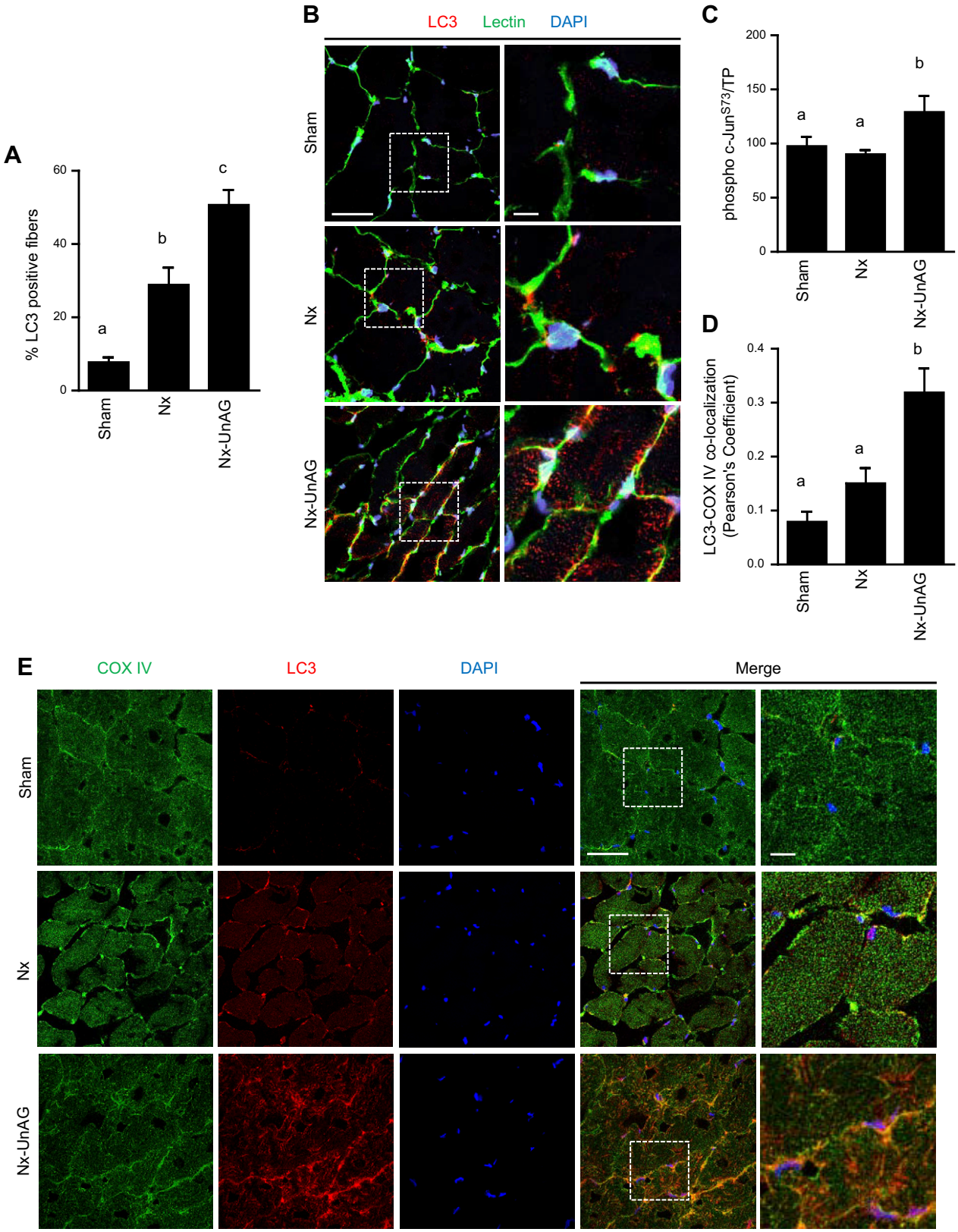

Figure 4. Autophagy and mitophagy in skeletal muscle. *A*, *B*) Gastrocnemius relative count of LC3-positive fibers (*A*) with representative images (*B*) showing lectin (green), LC3 (red), and nuclei (blue) in gastrocnemius muscle of Nx rats treated for 4 d with unacylated (UnAG) ghrelin treatment (200 μg, s.c. injection twice a day; scale bar, 30 μm). Enlargement of each picture is displayed alongside (scale bar, 6 μm; *B*). *C–E*) Muscle c-Jun^{S73} phosphorylation levels (*C*) and colocalization analysis by Pearson's correlation coefficient of mitochondrial marker COX IV (green), LC3 (red), and nuclei (blue) in muscle samples (scale bars, 50 and 10 μm; *D*) with representative images (*E*). Contrast and brightness settings are equal in all images. TP, total protein content. Different letters (*a–c*) indicate $P < 0.05$ between groups; means ± SEM, $n = 6$ per group.

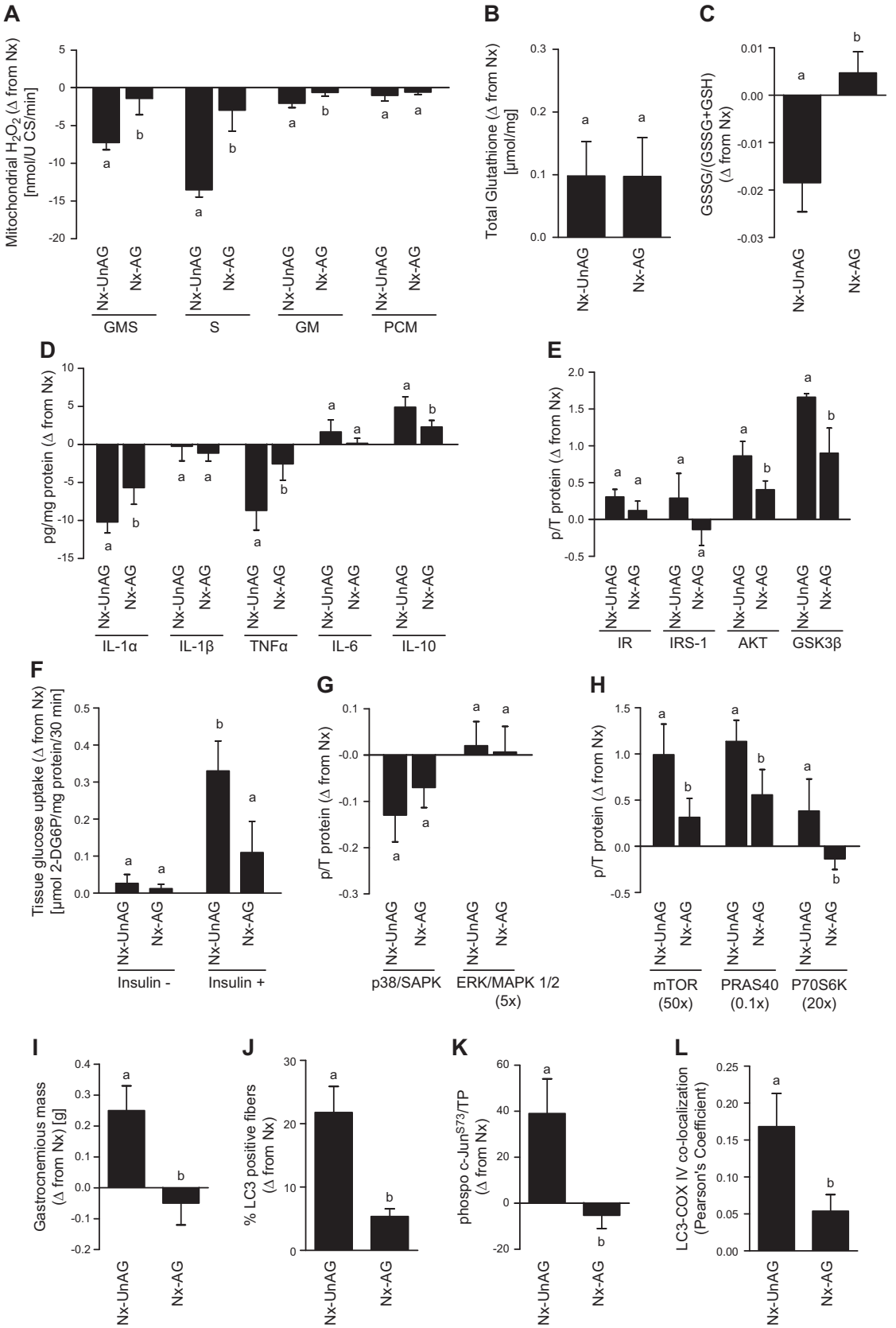

Figure 5. Differential impact of UnAG and AG on skeletal muscle metabolism in Nx rats. *A–F*) Effects of 4 d UnAG or AG ghrelin treatment (200 µg s.c. injection twice a day) in Nx rats on gastrocnemius muscle H_2O_2 production in intact isolated mitochondria with different respiratory substrates (*A*; GMS, glutamate + succinate + malate; S, succinate; GM, glutamate + malate; PCM, palmitoyl-L-carnitine + malate), total (*B*), and GSSG over total (*C*) tissue glutathione, tissue protein expression of IL-1α, IL-1β, TNF-α, IL-6, and IL-10 (*D*), relative phosphorylation of $IR^{Y1162/Y1163}$, $IRS\text{-}1^{S312}$, AKT^{S473}, and $GSK\text{-}3\beta^{S9}$ (*E*), and on extensor

(*continued on next page*)

UnAG activities are confirmed *in vitro* in C2C12 myotubes, and autophagy inhibition by genomic silencing abolishes UnAG-mediated effects on ROS production and insulin signaling in HUS-treated myotubes

To confirm that UnAG acts directly in muscle tissue, we performed *in vitro* experiments in C2C12 myotubes incubated with human uremic serum (HUS), thereby reproducing an established *in vitro* uremia model. In excellent agreement with *in vivo* findings (30, 31), HUS incubation resulted in higher mitochondrial ROS generation and globally reduced insulin signaling activation. Also consistent with *in vivo* findings, HUS also led to enhanced phosphorylation of p38/SAPK, although not that of MAPK/ERK. Addition of UnAG notably normalized mitochondrial ROS generation and insulin signaling as well as p38/SAPK activation in HUS-treated cells (**Fig. 6**). In agreement with *in vivo* differential effects for AG, all UnAG activities were unaffected by equimolar AG coincubation (Supplemental Fig. 4). In order to further determine the mechanistic role of UnAG-induced changes in autophagy, HUS-treated myotubes were incubated with UnAG in the absence or presence of siRNA against the key mediator of autophagosome formation ATG5. siRNA-mediated genomic silencing of ATG5 completely prevented the UnAG-induced decrease of mitochondrial ROS production as well as normalization of insulin signaling protein and p38/SAPK activating phosphorylation (Fig. 6).

DISCUSSION

The current results demonstrated the following: *1*) 4 d of UnAG administration normalizes nephrectomy-induced skeletal muscle mitochondrial ROS overproduction and catabolic abnormalities with reduced muscle weight; *2*) UnAG activities are confirmed in myotubes *in vitro* and are not reproduced by AG *in vivo*, thereby demonstrating that UnAG acts at least in part directly and independently of AG-regulated pathways; and *3*) UnAG enhances skeletal muscle mitophagy, and its effects are abolished *in vitro* by silencing of the autophagosome component ATG5, further demonstrating a direct role of mitophagy in mediating UnAG activities.

CKD-induced skeletal muscle metabolic abnormalities

The current combined *in vivo* and *in vitro* results demonstrate that skeletal muscle mitochondrial ROS overproduction is a novel CKD-induced alteration associated with catabolic abnormalities and loss of muscle mass (8, 44, 45). These findings are in excellent agreement with the emerging concept that kidney disease may induce a global increase in muscle ROS generation through yet unidentified biochemical mechanisms that likely involve accumulation of uremic toxins, such as indoxyl sulfate (1, 10). Our study further indicates a pivotal role of mitochondria in the onset of CKD-induced muscle oxidative stress; this conclusion is supported by normalized oxidized-to-total glutathione ratio, reflecting global tissue redox balance in the presence of normalized mitochondrial ROS production in UnAG-treated animals despite residual ROS overproduction from alternative sources. In addition, the study strongly suggests a primary role of mitochondrial ROS overproduction and oxidative stress in the onset of CKD-induced skeletal muscle inflammation and insulin resistance. This conclusion is consistent with the lack of normalization of inflammation and insulin signaling in the absence of mitochondrial ROS normalization after AG treatment *in vivo* or ATG5 silencing *in vitro*. Also, interestingly, we found a CKD-induced activation of p38/SAPK that paralleled global CKD-induced metabolic alterations. Effects of p38/SAPK on skeletal muscle homeostasis and anabolism are reportedly complex and include myogenesis, with a putative role in exercise-induced muscle hypertrophy (46, 47). Paradoxical p38/SAPK involvement in inflammation-induced muscle catabolic changes had been also notably reported in human CKD (38), and the current *in vivo* and *in vitro* findings are in excellent agreement with this concept, thereby confirming that lowering p38/SAPK activity could also contribute to ameliorate CKD-induced muscle catabolism.

UnAG metabolic activities

The study tested the following two hypotheses: first, that CKD-induced muscle metabolic abnormalities are ameliorated by UnAG administration; and second, that UnAG activities involve mitophagy activation. Consistent with these hypotheses, 4 d of UnAG treatment normalized tissue mitochondrial ROS overproduction, redox state, inflammation, and insulin action, as well as muscle mass. Activation of p38/SAPK in untreated CKD animals was also notably normalized by UnAG, thereby further supporting a relevant role of p38 in CKD-induced muscle catabolism. *In vitro* experiments including UnAG-AG coincubation as well as AG administration *in vivo* indicate that UnAG acts at least in part directly in muscle cells and independently of AG-regulated signaling pathways. UnAG activities in experimental CKD are notably in excellent agreement with our recent report that UnAG exerts antioxidative mitochondrial effects in healthy and obese rodent skeletal muscle (27). It should be pointed out that AG was reported to improve insulin signaling in healthy rat skeletal muscle (48) and was previously shown by us

digitorum longus muscle glucose uptake in presence or absence of insulin coincubation (*F*). *G–L*) Differential impact of UnAG or acylated (AG) ghrelin treatment on phosphorylation of p38/SAPK $^{T180/Y182}$, MAPK/ERK $1/2^{T185/Y187}$ (*G*), mTOR^{S2448}, PRAS40^{T246}, and P70S6K$^{T421/S424}$ (*H*) on gastrocnemius muscle mass (*I*), on relative count of LC3 positive fibers (*J*), on c-Jun^{S73} phosphorylation (*K*), and on colocalization of mitochondrial marker COX IV with LC3 (*L*) in gastrocnemius muscle samples. U CS, units of citrate synthase; GSH, reduced glutathione; p/T, phosphoprotein to total protein ratio; TP, total protein content. Different letters (*a–c*) indicate $P < 0.05$ between groups; means ± SEM, n = 6–10 per group.

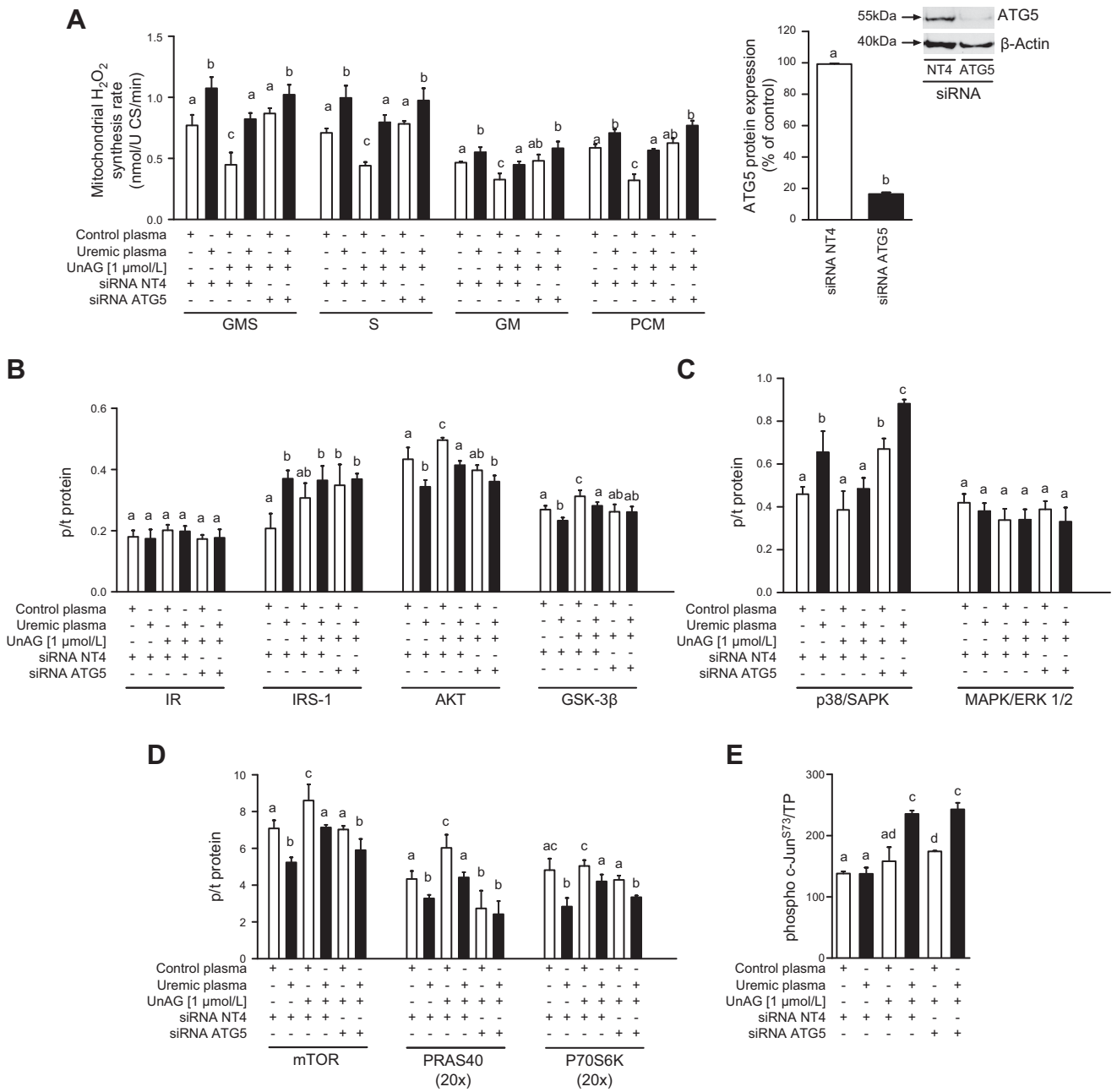

Figure 6. Impact of UnAG on autophagy in *in vitro* model of uremia. Effects of UnAG and of autophagy mediator ATG5 genomic silencing *vs.* nontargeting NT4 siRNA transfection, with representative blot, after 48 h incubation with 10% (v/v) plasma from uremic or control subjects on isolated mitochondria H_2O_2 synthesis rate with different respiratory substrates (*A*; GMS, glutamate + succinate + malate; S, succinate; GM, glutamate + malate; PCM, palmitoyl-L-carnitine + malate) and on relative phosphorylation of $IR^{Y1162/Y1163}$, IRS-1^{S312}, AKT^{S473}, GSK-$3\beta^{S9}$ (*B*), p38/SAPK $^{T180/Y182}$, MAPK/ERK $1/2^{T185/Y187}$ (*C*), $mTOR^{S2448}$, $PRAS40^{T246}$, $P70S6K^{T421/S424}$ (*D*), and c-Jun^{S73} (*E*) in C2C2 myotubes. U CS, units of citrate synthase; p/T, phosphoprotein to total protein ratio; TP, total protein content. Different letters (*a–c*) indicate $P < 0.05$ between groups; means ± SEM, $n = 3$ independent samples for each condition.

and others to improve insulin signaling and nutritional status in the nephrectomized rodent model (23). Orexigenic AG doses were, however, used in those studies (23), and enhancement of insulin signaling activation at AKT level was only observed in the presence of AG administration with enhanced food intake, and not in pair-feeding experiments. The current findings therefore collectively demonstrate that UnAG is a novel modulator of CKD-induced skeletal muscle metabolic abnormalities, and they provide a strong rationale for strategies involving UnAG administration to treat CKD-induced muscle metabolic complications. Identification of UnAG receptor or receptors and its downstream signaling pathways could provide further therapeutic targets and should be intensively pursued in future research.

Also in agreement with the working hypotheses, UnAG-treated animals had higher skeletal muscle autophagy activation at the mitochondrial level (mitophagy) compared to both untreated and sham-surgery groups.

UnAG effects on mitochondrial ROS production and insulin signaling were importantly abolished *in vitro* by coincubation with silencing RNA inhibiting the autophagosome component ATG5. On the other hand, less pronounced increments of autophagy markers were observed *in vivo* in skeletal muscle fibers from untreated nephrectomized animals only at the nonmitochondrial level. The current findings collectively demonstrate that selective activation of skeletal muscle mitophagy mediates at least in part the beneficial metabolic effects of UnAG, likely by reducing ROS overproduction by damaged mitochondria. It should be pointed out that the role of autophagy in the maintenance of muscle mass is still controversial (49), and whole-tissue autophagy activation is notably considered to be a relevant contributor to skeletal muscle loss through lysosomal protein degradation in acute and chronic disease conditions (2, 15). The current results in experimental CKD imply that localization of autophagic activities plays a key role in defining their impact on tissue oxidative stress and catabolic changes. A strong anticatabolic impact appears to be mediated by mitophagy activation, whereas enhanced autophagy at nonmitochondrial level might directly contribute to muscle depletion in untreated nephrectomized animals (14–16, 49). Interestingly, UnAG-induced improvement of high p38/SAPK phosphorylation was also dependent from its mitophagic activities, and this observation is indirectly in good agreement with the potential roles of oxidative stress and inflammation in MAPK/ERK-p38/SAPK activation in various models and conditions (50). Moreover, under the current experimental conditions, c-Jun, a transcription factor activated by autophagy/mitophagy-associated JNKs (41–43) and known to up-regulate the autophagosome regulator ATG-5 (40), was notably found to be selectively activated in UnAG-treated animals, suggesting its potential role as a target of UnAG activities and a contributor to UnAG-induced mitophagy activation both *in vivo* and directly *in vitro*. Identification of additional potential molecular pathways for autophagy activation also has a strong therapeutic potential and should be actively pursued in future investigations.

In summary, we demonstrated a novel role of UnAG to normalize a CKD-induced pattern of skeletal muscle mitochondrial dysfunction with high ROS production and tissue oxidative stress, catabolic abnormalities, and loss of muscle weight. UnAG skeletal muscle activities appear to be independent and direct, and they require stimulation of autophagy with selective mitochondrial localization (mitophagy). The current findings, taken together, indicate both UnAG and mitophagy to be potential novel treatments for CKD-induced skeletal muscle metabolic abnormalities leading to muscle wasting and its negative impact on patient morbidity and mortality. FJ

ACKNOWLEDGMENTS

The authors thank M. Stebel and R. Munaò (both from the University of Trieste), for excellent assistance in *in vivo* procedures; G. Spirito (University of Trieste) and A. Falcione (International Centre for Genetic Engineering and Biotechnology, Trieste, Italy) are acknowledged for their skillful technical assistance in *ex vivo* and *in vitro* experiments. This work was supported, in part, by the European Society for Clinical Nutrition and Metabolism (ESPEN) through a fellowship to G.G.C. Presented, in part, in abstract form at ESPEN congresses in 2015 and 2016. The authors declare no conflicts of interest.

AUTHOR CONTRIBUTIONS

G. Gortan Cappellari set up surgical procedures, performed surgery and experiments, researched and analyzed data, and contributed to study design and writing of the article; A. Semolic, G. Ruozi, and F. Bortolotti performed experiments and contributed to data analysis and discussion; P. Vinci and G. Guarnieri contributed to data discussion; D. Barbetta performed anaesthesia and guided perioperative therapy, provided care and pain control, and contributed to *in vivo* measurements and data discussion; M. Zanetti contributed to data discussion and reviewed and edited the article; M. Giacca contributed to design experiments, reviewed and discussed data, and reviewed and edited the article; and R. Barazzoni designed the study, reviewed data, wrote the article, and acts as guarantor for the article.

REFERENCES

1. Enoki, Y., Watanabe, H., Arake, R., Sugimoto, R., Imafuku, T., Tominaga, Y., Ishima, Y., Kotani, S., Nakajima, M., Tanaka, M., Matsushita, K., Fukagawa, M., Otagiri, M., and Maruyama, T. (2016) Indoxyl sulfate potentiates skeletal muscle atrophy by inducing the oxidative stress–mediated expression of myostatin and atrogin-1. *Sci. Rep.* **6**, 32084
2. Wang, X. H., and Mitch, W. E. (2014) Mechanisms of muscle wasting in chronic kidney disease. *Nat. Rev. Nephrol.* **10**, 504–516
3. Crowe, A. V., McArdle, A., McArdle, F., Pattwell, D. M., Bell, G. M., Kemp, G. J., Bone, J. M., Griffiths, R. D., and Jackson, M. J. (2007) Markers of oxidative stress in the skeletal muscle of patients on haemodialysis. *Nephrol. Dial. Transplant.* **22**, 1177–1183
4. Koppe, L., Pelletier, C. C., Alix, P. M., Kalbacher, E., Fouque, D., Soulage, C. O., and Guebre-Egziabher, F. (2014) Insulin resistance in chronic kidney disease: new lessons from experimental models. *Nephrol. Dial. Transplant.* **29**, 1666–1674
5. Stenvinkel, P., Heimbürger, O., Paultre, F., Diczfalusy, U., Wang, T., Berglund, L., and Jogestrand, T. (1999) Strong association between malnutrition, inflammation, and atherosclerosis in chronic renal failure. *Kidney Int.* **55**, 1899–1911
6. Filiopoulos, V., Hadjiyannakos, D., Takouli, L., Metaxaki, P., Sideris, V., and Vlassopoulos, D. (2009) Inflammation and oxidative stress in end-stage renal disease patients treated with hemodialysis or peritoneal dialysis. *Int. J. Artif. Organs* **32**, 872–882
7. Friedman, J. E., Dohm, G. L., Elton, C. W., Rovira, A., Chen, J. J., Leggett-Frazier, N., Atkinson, S. M., Jr., Thomas, F. T., Long, S. D., and Caro, J. F. (1991) Muscle insulin resistance in uremic humans: glucose transport, glucose transporters, and insulin receptors. *Am. J. Physiol.* **261**, E87–E94
8. Guarnieri, G., Zanetti, M., Vinci, P., Cattin, M. R., and Barazzoni, R. (2009) Insulin resistance in chronic uremia. *J. Ren. Nutr.* **19**, 20–24
9. Meyer, T. W., and Hostetter, T. H. (2007) Uremia. *N. Engl. J. Med.* **357**, 1316–1325
10. Nishikawa, M., Ishimori, N., Takada, S., Saito, A., Kadoguchi, T., Furihata, T., Fukushima, A., Matsushima, S., Yokota, T., Kinugawa, S., and Tsutsui, H. (2015) AST-120 ameliorates lowered exercise capacity and mitochondrial biogenesis in

the skeletal muscle from mice with chronic kidney disease *via* reducing oxidative stress. *Nephrol. Dial. Transplant.* **30**, 934–942

11. Sato, E., Mori, T., Mishima, E., Suzuki, A., Sugawara, S., Kurasawa, N., Saigusa, D., Miura, D., Morikawa-Ichinose, T., Saito, R., Oba-Yabana, I., Oe, Y., Kisu, K., Naganuma, E., Koizumi, K., Mokudai, T., Niwano, Y., Kudo, T., Suzuki, C., Takahashi, N., Sato, H., Abe, T., Niwa, T., and Ito, S. (2016) Metabolic alterations by indoxyl sulfate in skeletal muscle induce uremic sarcopenia in chronic kidney disease. *Sci. Rep.* **6**, 36618
12. Workeneh, B. T., and Mitch, W. E. (2010) Review of muscle wasting associated with chronic kidney disease. *Am. J. Clin. Nutr.* **91**, 1128S–1132S
13. Kovesdy, C. P., and Kalantar-Zadeh, K. (2009) Why is protein-energy wasting associated with mortality in chronic kidney disease? *Semin. Nephrol.* **29**, 3–14
14. Mizushima, N., and Komatsu, M. (2011) Autophagy: renovation of cells and tissues. *Cell* **147**, 728–741
15. Wang, D. T., Yang, Y. J., Huang, R. H., Zhang, Z. H., and Lin, X. (2015) Myostatin activates the ubiquitin–proteasome and autophagy–lysosome systems contributing to muscle wasting in chronic kidney disease. *Oxid. Med. Cell. Longev.* **2015**, 684965
16. Yao, Z., and Klionsky, D. J. (2016) An unconventional pathway for mitochondrial protein degradation. *Autophagy* **12**, 1971–1972
17. Ruozi, G., Bortolotti, F., Falcione, A., Dal Ferro, M., Ukovich, L., Macedo, A., Zentilin, L., Filigheddu, N., Gortan Cappellari, G., Baldini, G., Zweyer, M., Barazzoni, R., Graziani, A., Zacchigna, S., and Giacca, M. (2015) AAV-mediated *in vivo* functional selection of tissue-protective factors against ischaemia. *Nat. Commun.* **6**, 7388
18. Sarparanta, J., García-Macia, M., and Singh, R. (2017) Autophagy and mitochondria in obesity and type 2 diabetes. *Curr. Diabetes Rev.* **13**, 352–369
19. Chen, C. Y., Asakawa, A., Fujimiya, M., Lee, S. D., and Inui, A. (2009) Ghrelin gene products and the regulation of food intake and gut motility. *Pharmacol. Rev.* **61**, 430–481
20. Nakazato, M., Murakami, N., Date, Y., Kojima, M., Matsuo, H., Kangawa, K., and Matsukura, S. (2001) A role for ghrelin in the central regulation of feeding. *Nature* **409**, 194–198
21. Müller, T. D., Nogueiras, R., Andermann, M. L., Andrews, Z. B., Anker, S. D., Argente, J., Batterham, R. L., Benoit, S. C., Bowers, C. Y., Broglio, F., Casanueva, F. F., D'Alessio, D., Depoortere, I., Geliebter, A., Ghigo, E., Cole, P. A., Cowley, M., Cummings, D. E., Dagher, A., Diano, S., Dickson, S. L., Diéguez, C., Granata, R., Grill, H. J., Grove, K., Habegger, K. M., Heppner, K., Heiman, M. L., Holsen, L., Holst, B., Inui, A., Jansson, J. O., Kirchner, H., Korbonits, M., Laferrère, B., LeRoux, C. W., Lopez, M., Morin, S., Nakazato, M., Nass, R., Perez-Tilve, D., Pfluger, P. T., Schwartz, T. W., Seeley, R. J., Sleeman, M., Sun, Y., Sussel, L., Tong, J., Thorner, M. O., van der Lely, A. J., van der Ploeg, L. H., Zigman, J. M., Kojima, M., Kangawa, K., Smith, R. G., Horvath, T., and Tschöp, M. H. (2015) Ghrelin. *Mol. Metab.* **4**, 437–460
22. Barazzoni, R., Gortan Cappellari, G., Zanetti, M., and Guarnieri, G. (2012) Ghrelin and muscle metabolism in chronic uremia. *J. Ren. Nutr.* **22**, 171–175
23. Barazzoni, R., Zhu, X., Deboer, M., Datta, R., Culler, M. D., Zanetti, M., Guarnieri, G., and Marks, D. L. (2010) Combined effects of ghrelin and higher food intake enhance skeletal muscle mitochondrial oxidative capacity and AKT phosphorylation in rats with chronic kidney disease. *Kidney Int.* **77**, 23–28
24. Broglio, F., Arvat, E., Benso, A., Gottero, C., Muccioli, G., Papotti, M., van der Lely, A. J., Deghenghi, R., and Ghigo, E. (2001) Ghrelin, a natural GH secretagogue produced by the stomach, induces hyperglycemia and reduces insulin secretion in humans. *J. Clin. Endocrinol. Metab.* **86**, 5083–5086
25. Barazzoni, R., Bosutti, A., Stebel, M., Cattin, M. R., Roder, E., Visintin, L., Cattin, L., Biolo, G., Zanetti, M., and Guarnieri, G. (2005) Ghrelin regulates mitochondrial–lipid metabolism gene expression and tissue fat distribution in liver and skeletal muscle. *Am. J. Physiol. Endocrinol. Metab.* **288**, E228–E235; Erratum **291**, E428
26. Barazzoni, R., Zanetti, M., Stulle, M., Mucci, M. P., Pirulli, A., Dore, F., Panzetta, G., Vasile, A., Biolo, G., and Guarnieri, G. (2008) Higher total ghrelin levels are associated with higher insulin-mediated glucose disposal in non-diabetic maintenance hemodialysis patients. *Clin. Nutr.* **27**, 142–149
27. Gortan Cappellari, G., Zanetti, M., Semolic, A., Vinci, P., Ruozi, G., Falcione, A., Filigheddu, N., Guarnieri, G., Graziani, A., Giacca, M., and Barazzoni, R. (2016) Unacylated ghrelin reduces skeletal muscle reactive oxygen species generation and inflammation and prevents high-fat diet–induced hyperglycemia and whole-body insulin resistance in rodents. *Diabetes* **65**, 874–886
28. Tong, X. X., Wu, D., Wang, X., Chen, H. L., Chen, J. X., Wang, X. X., Wang, X. L., Gan, L., Guo, Z. Y., Shi, G. X., Zhang, Y. Z., and Jiang, W. (2012) Ghrelin protects against cobalt chloride–induced hypoxic injury in cardiac H9c2 cells by inhibiting oxidative stress and inducing autophagy. *Peptides* **38**, 217–227
29. Holecek, M. (2012) Muscle wasting in animal models of severe illness. *Int. J. Exp. Pathol.* **93**, 157–171
30. Martinez Cantarin, M. P., Keith, S. W., Waldman, S. A., and Falkner, B. (2014) Adiponectin receptor and adiponectin signaling in human tissue among patients with end-stage renal disease. *Nephrol. Dial. Transplant.* **29**, 2268–2277
31. Folli, F., Sinha, M. K., Brancaccio, D., and Caro, J. F. (1986) Insulin resistance in uremia: *in vitro* model in the rat liver using human serum to study mechanisms. *Metabolism* **35**, 989–998
32. Lovric, J., Mano, M., Zentilin, L., Eulalio, A., Zacchigna, S., and Giacca, M. (2012) Terminal differentiation of cardiac and skeletal myocytes induces permissivity to AAV transduction by relieving inhibition imposed by DNA damage response proteins. *Mol. Ther.* **20**, 2087–2097
33. Ryter, S. W., Koo, J. K., and Choi, A. M. (2014) Molecular regulation of autophagy and its implications for metabolic diseases. *Curr. Opin. Clin. Nutr. Metab. Care* **17**, 329–337
34. Barazzoni, R., Zanetti, M., Gortan Cappellari, G., Semolic, A., Boschelle, M., Codarin, E., Pirulli, A., Cattin, L., and Guarnieri, G. (2012) Fatty acids acutely enhance insulin-induced oxidative stress and cause insulin resistance by increasing mitochondrial reactive oxygen species (ROS) generation and nuclear factor-κB inhibitor (IκB)-nuclear factor-κB (NFκB) activation in rat muscle, in the absence of mitochondrial dysfunction. *Diabetologia* **55**, 773–782
35. Yamamoto, N., Kawasaki, K., Kawabata, K., and Ashida, H. (2010) An enzymatic fluorimetric assay to quantitate 2-deoxyglucose and 2-deoxyglucose-6-phosphate for *in vitro* and *in vivo* use. *Anal. Biochem.* **404**, 238–240
36. Workeneh, B. T., Rondon-Berrios, H., Zhang, L., Hu, Z., Ayehu, G., Ferrando, A., Kopple, J. D., Wang, H., Storer, T., Fournier, M., Lee, S. W., Du, J., and Mitch, W. E. (2006) Development of a diagnostic method for detecting increased muscle protein degradation in patients with catabolic conditions. *J. Am. Soc. Nephrol.* **17**, 3233–3239
37. Gao, X., Wu, J., Dong, Z., Hua, C., Hu, H., and Mei, C. (2010) A low-protein diet supplemented with ketoacids plays a more protective role against oxidative stress of rat kidney tissue with 5/6 nephrectomy than a low-protein diet alone. *Br. J. Nutr.* **103**, 608–616
38. Verzola, D., Bonanni, A., Sofia, A., Montecucco, F., D'Amato, E., Cademartori, V., Parodi, E. L., Viazzi, F., Venturelli, C., Brunori, G., and Garibotto, G. (2017) Toll-like receptor 4 signalling mediates inflammation in skeletal muscle of patients with chronic kidney disease. *J. Cachexia Sarcopenia Muscle* **8**, 131–144
39. Li, Y. P., Chen, Y., John, J., Moylan, J., Jin, B., Mann, D. L., and Reid, M. B. (2005) TNF-alpha acts *via* p38 MAPK to stimulate expression of the ubiquitin ligase atrogin1/MAFbx in skeletal muscle. *FASEB J.* **19**, 362–370
40. Byun, J. Y., Yoon, C. H., An, S., Park, I. C., Kang, C. M., Kim, M. J., and Lee, S. J. (2009) The Rac1/MKK7/JNK pathway signals upregulation of Atg5 and subsequent autophagic cell death in response to oncogenic Ras. *Carcinogenesis* **30**, 1880–1888
41. Jaeschke, A., Karasarides, M., Ventura, J. J., Ehrhardt, A., Zhang, C., Flavell, R. A., Shokat, K. M., and Davis, R. J. (2006) JNK2 is a positive regulator of the cJun transcription factor. *Mol. Cell* **23**, 899–911
42. Wei, Y., Pattingre, S., Sinha, S., Bassik, M., and Levine, B. (2008) JNK1-mediated phosphorylation of Bcl-2 regulates starvation-induced autophagy. *Mol. Cell* **30**, 678–688

43. Zhang, Q., Kuang, H., Chen, C., Yan, J., Do-Umehara, H. C., Liu, X. Y., Dada, L., Ridge, K. M., Chandel, N. S., and Liu, J. (2015) The kinase Jnk2 promotes stress-induced mitophagy by targeting the small mitochondrial form of the tumor suppressor ARF for degradation. *Nat. Immunol.* **16**, 458–466
44. Zanetti, M., Barazzoni, R., and Guarnieri, G. (2008) Inflammation and insulin resistance in uremia. *J. Ren. Nutr.* **18**, 70–75
45. Barazzoni, R. (2004) Skeletal muscle mitochondrial protein metabolism and function in ageing and type 2 diabetes. *Curr. Opin. Clin. Nutr. Metab. Care* **7**, 97–102
46. Keren, A., Tamir, Y., and Bengal, E. (2006) The p38 MAPK signaling pathway: a major regulator of skeletal muscle development. *Mol. Cell. Endocrinol.* **252**, 224–230
47. Yu, M., Stepto, N. K., Chibalin, A. V., Fryer, L. G., Carling, D., Krook, A., Hawley, J. A., and Zierath, J. R. (2003) Metabolic and mitogenic signal transduction in human skeletal muscle after intense cycling exercise. *J. Physiol.* **546**, 327–335
48. Barazzoni, R., Zanetti, M., Cattin, M. R., Visintin, L., Vinci, P., Cattin, L., Stebel, M., and Guarnieri, G. (2007) Ghrelin enhances *in vivo* skeletal muscle but not liver AKT signaling in rats. *Obesity (Silver Spring)* **15**, 2614–2623
49. Sandri, M. (2013) Protein breakdown in muscle wasting: role of autophagy–lysosome and ubiquitin–proteasome. *Int. J. Biochem. Cell Biol.* **45**, 2121–2129
50. Kim, E. K., and Choi, E. J. (2010) Pathological roles of MAPK signaling pathways in human diseases. *Biochim. Biophys. Acta* **1802**, 396–405

Accepted for publication July 17, 2017.